Performance of ERA5 data in retrieving Precipitable Water Vapour over East African tropical region

Ssenyunzi, Richard Cliffe; Oruru, Bosco; D'ujanga, Florence Mutonyi; Realini, Eugenio; Barindelli, Stefano; Tagliaferro, Giulio; von Engeln, Axel; van de Giesen, Nick

DOI
10.1016/j.asr.2020.02.003

Publication date
2020

Document Version
Final published version

Published in
Advances in Space Research

Citation (APA)
Ssenyunzi, R. C., Oruru, B., D'ujanga, F. M., Realini, E., Barindelli, S., Tagliaferro, G., von Engeln, A., & van de Giesen, N. (2020). Performance of ERA5 data in retrieving Precipitable Water Vapour over East African tropical region. *Advances in Space Research*, *65*(8), 1877-1893. https://doi.org/10.1016/j.asr.2020.02.003

Available online at www.sciencedirect.com

ScienceDirect

Advances in Space Research 65 (2020) 1877–1893

ADVANCES IN SPACE RESEARCH (a COSPAR publication)

www.elsevier.com/locate/asr

Performance of ERA5 data in retrieving Precipitable Water Vapour over East African tropical region

Richard Cliffe Ssenyunzi [a,b,*], Bosco Oruru [a], Florence Mutonyi D'ujanga [a], Eugenio Realini [c], Stefano Barindelli [d], Giulio Tagliaferro [e], Axel von Engeln [f], Nick van de Giesen [g]

[a] Department of Physics, Makerere University, P.O. Box 7062, Kampala, Uganda
[b] Department of Physics, Busitema University, P.O. Box 236, Tororo, Uganda
[c] Geomatics Research & Development srl, Via Cavour 2, 22074 Lomazzo, Italy
[d] Department of Civil and Environmental Engineering, Politecnico di Milano, P.zza Leonardo da Vinci 32, 20133 Milano, Italy
[e] Geomatics Research & Development srl, Via Cavour 2, 22074 Lomazzo, Italy
[f] EUMETSAT, Eumetsat Allee 1, D-64295 Darmstadt, Germany
[g] Water Management, Civil Engineering and Geosciences TU Delft, The Netherlands, P.O. Box 5048, 2600 GA Delft, Netherlands

Received 18 June 2019; received in revised form 25 January 2020; accepted 2 February 2020
Available online 13 February 2020

Abstract

The accuracy of surface meteorological measurements is vital to derive accurate Global Positioning System (GPS) Precipitable Water Vapour (PWV) data. However, in absence of surface meteorological data, data from Numerical Weather Prediction Models (NWP) are used. The accuracy of these models varies depending on the model, region, season and other climatic conditions. In this study, GPS data for derivation of PWV is collected from 13 geodetic permanent stations for the years 2013 to 2016. Five out of 13 GPS stations are equipped with meteorological sensors. The interpolated European Centre for Medium-Range Weather Forecasts (ECMWF) 5th Re-Analysis (ERA5) dataset at these locations is first validated using the meteorological data from these sensors. The assessment shows that the average root mean square errors (RMSE) of surface pressure and temperature values are about 0.72 hPa and 1.04 K respectively. PWV determined also requires information on the weighted mean temperature (T_m); the T_m at the 13 GPS stations was also evaluated using three methods: the temperature and humidity profiles from ERA5 (ERA5 T_m), as well as the T_m derived from Bevis and Yao T_m - T_s relationships. The T_m derived from ERA5 was used as a reference to assess the errors of the Bevis and Yao T_m. The comparisons show that the average RMSE values of T_m derived from the two methods are 2.05 K and 2.02 K respectively. The GPS PWVs calculated using the ERA5 interpolated data (GPS ERA5 PWV) were compared to GPS PWV calculated using the sensor meteorological data (GPS MET PWV) at the 5 stations. The GPS ERA5 PWV values were used as the reference. The RMSE values of the two PWV datasets are in the range of 0.19 mm to 0.90 mm with overall average value of 0.44 mm. Also the computed ERA5 PWV data are compared to GPS ERA5 PWV at the 13 stations. ERA5 PWV values were used as the reference and the RMS errors of the two PWV values are in the range 1.35 mm to 2.25 mm with the overall average value of 1.66 mm. Regarding the seasonal variations, the stations between latitudes 4 °S and 4 °N and latitudes 12 °S to 4 °S have the highest PWV values in spring and summer while the lowest values occur in summer and winter respectively.

Keywords: ECMWF; NWP; GNSS; ERA5; PWV

* Corresponding author at: Department of Physics, Makerere University, P.O. Box 7062, Kampala, Uganda.
E-mail address: ssecliffe@gmail.com (R.C. Ssenyunzi).

https://doi.org/10.1016/j.asr.2020.02.003
0273-1177/

1. Introduction

Atmospheric water vapour is an environmentally significant part of the atmosphere with approximately 99% of it contained in the troposphere and 1% in the stratosphere. The main source of water vapour is the evaporation from water bodies and transpiration by plants and its content depends on the local geographic conditions and meteorological phenomena. It exhibits spatial–temporal variability (Namaoui et al., 2017; Alshawaf et al., 2017). It is one of the fundamental greenhouse gases which contributes to the Earth's natural greenhouse effect which keeps the surface of the Earth warmer and liveable (Wang et al., 2017). The condensation of water vapour to liquid or ice phase is responsible for clouds, rain, snow, and other precipitation, all of which count among the most significant elements of weather (Moustafa, 1992). As water vapour moves in the atmosphere, it redistributes energy or latent heat of vaporization, which is released through condensation (Li et al., 2014). This is one of the most important conditions in the atmospheric energy budget on both local and global scales and is an important climate variable in most major weather events such as tropical cyclones and severe thunderstorms (Sharifi et al., 2015; Zhang et al., 2018). Therefore, understanding and monitoring the quantity and distribution of atmospheric water vapour, and the effects on atmospheric radiation and circulation, is vital in the analysis and forecast of short and long-term changes in climate.

The measurements of water vapour may be expressed in terms of precipitable water vapour (PWV), which is the total atmospheric water vapour contained in a vertical air column of unit area from the Earth's surface to the top of the atmosphere (Alshawaf et al., 2017). The spatial and temporal variability of water vapour makes it a very difficult parameter to measure (Namaoui et al., 2017). The introduction of radiosonde in 1940s (Durre et al., 2006), partly improved the availability of precipitable water vapour data, albeit at very low spatial and temporal resolutions. Currently, many observational techniques are being used in the measurement of the precipitable water vapour measurements. These include radiosondes, ground-based upward-looking radiometry, satellite-based downward-looking radiometry (Bevis et al., 1992), Light Detection and Ranging (LIDAR) systems (Gerding et al., 2004; Kuwahara et al., 2008), GPS and sun photometers (Bock et al., 2007b; Campanelli et al., 2018). Also, algorithms and techniques to derive the PWV from temperature measurements by infrared radiometers have been considered (Maghrabi, 2009; Maghrabi and Clay, 2010). However, some of these techniques have limitations which have affected the accuracy of water vapour measurements. Some measurement techniques such as LIDAR are too expensive and are missing in most parts of Africa, including East Africa. Others such as space-based instruments have low resolution, while the radiosondes offer limited coverage.

Ground-based GPS receivers are capable of providing PWV with a high temporal and spatial resolution (Yunck et al., 2000). Compared to other techniques, they offer a number of advantages which include the capability to provide continuous data of good quality under all weather conditions and above all surfaces (Hagemann et al., 2003). Since 1992, Global Positioning System (GPS) has been presented as an efficient meteorological tool (Bevis et al., 1992) and is being increasingly used for estimating atmospheric parameters such as precipitable water vapour (Gendt et al., 2004; Alshawaf et al., 2015). The GPS PWV observations have many applications, including calibrating or validating water vapour observations generated from other sources such as radiosonde observations and satellite water vapour observations with high accuracy (Köpken, 2001; Bock et al., 2010; Buehler et al., 2012), monitoring climate change (Yuan et al., 1993), and assimilation into numerical weather prediction models in order to increase on both short-term and long-term weather prediction accuracy (Vedel and Huang, 2004; Gendt et al., 2004; Bock et al., 2005; Bennitt and Jupp, 2012).

Although studies on estimating PWV using ground-based GPS measurements has been done in Africa, e.g. Bock et al. (2007a), Combrink et al. (2004), Mengistu et al. (2015), Abraha et al. (2015), Namaoui et al. (2017), the East African tropical region has not yet been addressed due to limited GPS networks, lack of accurate and reliable surface meteorological data and other ground-based atmospheric observing systems, as well as large data gaps, as also observed for other regions of Africa by King et al. (2003) and Bock et al. (2007b). This, therefore, calls for an in-depth study of water vapour estimations in the East African tropical region, because the studies carried out over Africa such as Bock et al. (2007b), used scattered GPS receiver stations which makes these studies hardly represent the whole continent. Also the content of the atmospheric water vapour varies greatly in magnitude and distribution in a given location depending on the season, latitude, surface altitude and whether the atmosphere is located above land or water. Africa, however, has recently seen an increase in the GPS ground receiver sites for geodetic studies for some regions such as northern Africa and the African Monsoon Multidisciplinary Analyses (AMMA) project over West Africa (Bock et al., 2007b; Koulali et al., 2011). East African tropical region has also recently benefited from the AfricaArray (AA), which has created a multidisciplinary research network for the broader Earth science community, by installing continuous GPS instruments fitted with meteorological (MET) sensors.

The estimation of PWV using GPS technology, begins with estimating the zenith total delay (ZTD). Using GPS processing software, ZTD can be precisely estimated depending on satellite geometry, quality of the mapping function, and data availability (Luo et al., 2013). The ZTD can be divided into two components: a hydrostatic component mainly caused by dry gases of air (ZHD),

and a non-hydrostatic (wet) component (ZWD) due to water vapour (Davis et al., 1985). For GPS signals, the tropospheric delay can be over 2 m at the zenith and it increases to more than 10 m for an elevation angle of 10° (Luo et al., 2013). The ZHD contributes approximately 90% of the magnitude of the ZTD and since it can be estimated fairly accurate, the ZWD in this study will be estimated as unknown parameter as cited in Dach et al. (2015) and Herring et al. (2015). The accuracy of PWV depends on the accuracy of estimated ZWD, which also depends on the accuracy of ZHD. However, the accuracy of ZHD highly depends upon the accuracy of the surface meteorological measurements, as well as the selected ZHD model. Although the East African tropical region has seen an increase in the GPS ground receiver sites, estimation of PWV is still a challenge due to limited or lack of accurate and reliable surface meteorological data and, as well, large data gaps in the already scarce data. Lack of accurate meteorological measurements affects the accuracy of the Global Positioning System (GPS) Precipitable Water Vapour (PWV). If surface meteorological data are not available, data from Numerical Weather Prediction Models (NWP), e.g. the European Centre for Medium-Range Weather Forecasts (ECMWF) (Alshawaf et al., 2017), or alternatively, empirical meteorological models such as Global Pressure and Temperature (GPT) (Boehm et al., 2007), may be applied. However, the accuracies of these models vary depending on the model, region, season and other climatic conditions. This therefore led to a study to assess the performance of ECMWF pressure with respect to available surface pressure observations in estimating the PWV from GPS data over the East African tropical region. This study will then assess whether ECMWF model level data can be applied to other areas without any surface meteorological data in estimating the PWV from GPS. The complex terrain of this region, unique from the rest of Africa also motivated the study to assess the performance of the earlier ECMWF re-analysis PWV with respect to coincident measurements from GPS. This is because several studies e.g. (Bock et al., 2005; Bock et al., 2007b; Koulali et al., 2011) have shown that ERA-Interim PWV has a good agreement elsewhere in the African continent with different terrain as compared to the East African tropical region.

The accuracy of the estimated Precipitable Water Vapor (PWV) from ground-based GPS has been investigated by many studies outside the African continent. The Root Mean Squares (RMS) of GPS PWV with respect to other independent observations has been reported for many countries/regions such as North America with about 2 mm, Europe and Australia, with about 2.6 mm at global International GPS Service (IGS) stations, 3.7 mm in Japan (Ohtani and Naito, 2000; Li et al., 2003; Gendt et al., 2004; Dietrich et al., 2004; Deblonde et al., 2005; Sibylle et al., 2010) as also cited by Sharifi et al. (2015) and 1.5 mm for Tehran (Sharifi et al., 2015). However, the accuracies of GPS PWV in some parts of Africa have also been investigated by comparison studies of GPS PWV with other independent observations. For instance, Bock et al. (2007b) used some scattered GPS receiver stations over Africa and compared them to 40-year ECMWF Re-Analysis (ERA-40) (an earlier re-analysis by ECMWF) and National Centers for Environmental Prediction reanalysis 2 (NCEP2) model simulations. A good agreement between ERA-40 PWV and GPS PWV at some GPS sites in western and northern Africa was found. Also, a study by Bock et al. (2011) found a relatively good agreement between GPS PWV and ERA-Interim PWV with respect to those between GPS PWV and other reanalyses such as NCEP2 over Western Africa. Generally, ERA-Interim PWV has been found to have a good agreement with GPS PWV in some regions of the African continent (Bock et al., 2005; Bock et al., 2007b; Koulali et al., 2011) of less complex topography compared to East African tropical region. However similar studies in more topographically complex regions similar to the East African tropical region have been carried out e.g. by Mengistu et al. (2015). From the comparison between GPS and ERA-Interim PWV over Ethiopian GPS stations, the study showed differences in the magnitude and sign of bias of ERA-Interim with respect to GPS PWV from station to station. Also, a comparison between GPS and ERA-Interim in Algeria showed a large difference of 4 mm in the highlands region and this was linked to the topography differences (Namaoui et al., 2017).

In this study, a network of 13 GPS stations equipped with dual-frequency receivers, 5 of which are equipped with meteorological sensors were used and data from each station were processed independently in Precise Point Positioning (PPP) mode to estimate ZTD from which PWV is derived. The performance of the ECMWF model level data and the available surface pressure observations in estimating the PWV from this network of ground-based GPS receivers in East African tropical region (Fig. 1) is analysed. Also the performance of GPS PWV and the ERA5 PWV from ECMWF is analysed.

2. Data and methodology

2.1. Area of study

The area of study lies within the latitude range 12 °S to 4 °N and longitude range 28 °E to 44 °E, which is part of the East African tropical region. It covers Kenya, Rwanda, Tanzania, and Uganda, which are also part of the Great Lakes region, neighbouring the Indian Ocean (Fig. 1). The East African tropical region partly covers the highest and the lowest points of the African continent. It is a region of strong elevation gradients with diverse topographical environments. Between 10 °S and 4 °N, lies the East African Highlands following the eastern and the western Rift valleys. These include the Kenya Highlands, at an average elevation of 1,500–2,500 m flanked by two highest Africa's mountains which include Mt. Kenya at an elevation of 5,199 m and Mt. Kilimanjaro at 5,895 m.

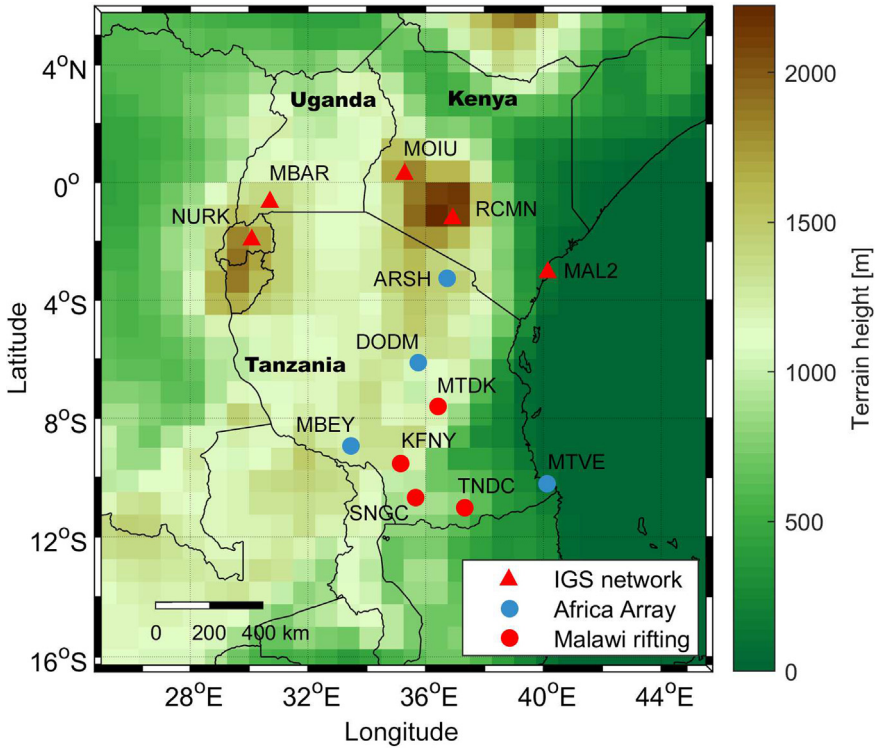

Fig. 1. Map of East Africa showing the GPS stations.

The region is also occupied by the western Rift Mountains with peaks above 3,000 m, among which Mountain Rwenzori at an elevation of 5,109 m. These highlands have a major impact on the regional climate (Slingo et al., 2005). The Eastern Africa tropical region exhibits a number of large water bodies, including Lake Albert (5,300 km^2), Lake Edward, Lake Kivu, Lake Tanganyika (32,900 km^2) and Lake Victoria (68,800 km^2 - the second largest freshwater Lake in the world), which are also important regulators for climate in the region (Thiery et al., 2015). For example, Lake Victoria drives Land-Lake breezes, which explains the convective activity over the Lake. The region is also dominated by rainfall tropical forests across parts of Kenya, Tanzania, and Uganda, often on steep slopes.

Being crossed by the equator, the Eastern Africa tropical region is directly affected by seasonal changes in the Hadley circulation with a twice-a-year migration of the Intertropical Convergence Zone (ITCZ) (Nicholson, 1996). This migration is accompanied by a change in the direction of the wind, from a northerly direction in boreal winter to a southerly direction in boreal summer, demonstrating the nature of monsoons. For the region between 4 °S and 4 °N, temperatures vary seasonally by not more than 5 °C, with the smallest range less than 2 °C occurring along the equator. In this region, highest temperatures are generally experienced in February and March before the main rains, while lowest temperatures are experienced in July and August, during the relatively dry cloudy season. The sea influence makes minimum temperatures along the coast relatively higher between 18 and 22 °C than inland 10.4 °C (Camberlin, 2018).

These are single-peak regimes for mostly the region between 12 °S and 4 °S and double-peak between 4 °S and 4 °N (Fig. 1). The region with single-peak regimes has a summer maximum corresponding to the ITCZ because of its location in the Southern hemisphere, with relatively heavy rainfall amounts from November to April (Camberlin, 2018).

The region which exhibits double-peak regimes receives rains in the transition seasons of March-April-May (MAM) and October-November-December (OND). The MAM season is called the long rains and OND referred to as short rains season. The lower rainfall amounts are found in the OND season as compared to the MAM season due to the Western Indian Ocean sea-surface temperature (SST) being lower in OND. This results in a drier, more stable atmosphere (Yang et al., 2015) and an equatorial westerly flow from the western to the eastern Indian Ocean associated with moisture (Camberlin, 2018). The OND rains increase when easterlies are stronger (Camberlin, 1997), resulting in the eastern side being wetter than in MAM, where more rain is linked to westerly anomalies. The MAM and OND seasons are separated by two dry seasons, of which the boreal summer between June and September is the longest and driest. The boreal summer dryness is caused by stable southeasterlies (Yang et al., 2015) and over a third of the rainfall maximum is found in this season as a due to presence of mid-tropospheric

moist westerlies and a low pressure anomaly (Davies et al., 1985).

Therefore land surface heterogeneity arising from the contrasted topography and the presence of major water bodies accounts for a number of local and regional scale winds, of great importance to rainfall distribution in the region. Also the complex terrain of this region, unique from the rest of Africa, results in a vast diversity of climatic conditions that steer a wide range of vegetation landscapes, biodiversity and human occupations.

2.2. Meteorological parameters

The set of meteorological parameters applied in this study consists of temperature and pressure from surface observation and the ECMWF model (Table 1). Surface pressure and temperature data with a sampling interval of 5 min (300 s) were obtained from ftp://data-out.unavco.org/pub/rinex/met/. They were measured by Vaisala HMP45A-P and WXT520 sensor models with pressure and temperature accuracy of 0.1 hPa and 0.2 °C, respectively. The height difference between the meteorological sensors and GPS receiver of each station ranged between −3.4 m and 0.8 m where a negative difference means the sensor height is below the GPS station height.

Out of the 13 GPS stations used in this study, only 5 stations (Arusha (ARSH), Dodoma (DODM), Mbeya (MBEY), Mtwara (MTVE) and Kigali (NURK)) are equipped with meteorological sensors. These stations are homogeneously distributed in the area under study, with stations ARSH and NURK located in the region characterized by a bimodal rainfall distribution and stations MBEY, DODM and MTVE, located in region characterized by unimodal rainfall distribution. The altitude range among the five stations is from −11.4 m to 1700.5 m. This altitude range covers 11 GPS stations with the exception of MOIU located at 2201.5 m above sea level and MAL2 at −20.9 m below sea level. Therefore, the 5 stations represent well the region under study.

Although the period of study is from 2013–2016, depending on the available data, the surface meteorological data available for the stations is only between 2013 to 2015.

2.3. ERA5 Reanalysis data

The pressure, temperature and humidity values were also obtained from the ERA5 reanalysis data as explained below.

ERA5 is the latest generation of ECMWF global atmospheric reanalysis from 1979 to present, produced by the ECMWF (Hersbach and Dee, 2016). In this study, the horizontal resolution of 0.25 ° × 0.25 ° is applied. The model has a vertical dimension of 137 model levels with the model top about 80 km, and 6 h temporal resolution.

A more detailed description of how model levels should be interpreted is available in the IFS documentation Part III- chapter 2 available at: https://www.ecmwf.int/sites/default/files/.

The geometric altitudes were calculated according to Mahoney (2001) and Lewis (2007). Vertical profiles at the station location are extracted from the gridded ERA5 fields by bilinear interpolation between the nearest 4 grid points. The PWV is calculated from the available specific humidity, pressure and temperature profiles:

$$PWV = \frac{1}{\rho_w g}\int_{Ps}^{0} q(P)dP \tag{1}$$

where ρ_w is the water density (1000 kgm^{-3}), g is the gravitational acceleration at the station model level altitude, $q(P)$ is the mixing ratio (g/kg) of water vapour.

The station altitude can be below the lowest model level of ECMWF since ECMWF only represents the data for the grid box; in that case, the profiles are linearly extrapolated. The height differences between GPS stations and interpolated nearest model grid points in this study, range from −582.20 m to +184.44 m, where a negative difference means GPS height is below the model surface as shown in Table 1.

Table 1
GPS stations coordinates. The column dz is the difference in altitude between the GPS station and lowest ECMWF model level.

Staion Id and City	Country	Longitude (E) degrees	Latitude (N) degrees	Ellipsoidal height (m)	dz (m)
ARSH (Arusha)	Tanzania	36.698	−3.387	1345.161	−62.59
DODM (Dodoma)	Tanzania	35.748	−6.187	1122.595	6.09
KFNY (Kifanya)	Tanzania	35.103	−9.547	1714.834	161.97
MAL2 (Malindi)	Kenya	40.194	−2.996	−20.937	−39.41
MBAR (Mbarara)	Uganda	30.738	−0.602	1337.530	−51.92
MBEY (Mbeya)	Tanzania	33.459	−8.912	1700.514	−57.96
MOIU (Eldoret)	Kenya	35.290	0.288	2201.511	13.43
MTDK (Mtandika)	Tanzania	36.421	−7.544	548.175	−582.20
MTVE (Mtwara)	Tanzania	40.166	−10.260	−11.414	−58.36
NURK (Kigali)	Rwanda	30.090	−1.945	1483.809	−60.87
RCMN (Nairobi)	Kenya	36.894	−1.221	1591.967	−87.28
SNGC (Songea)	Tanzania	35.673	−10.690	1181.221	184.44
TNDC (Tunduru)	Tanzania	37.341	−11.063	672.948	95.42

2.4. Determination of PWV from GPS data

Fig. 1 and Table 1 show the geographical locations of the selected GPS stations from which data are collected to obtain PWV. All the stations are equipped with dual-frequency receivers; some have an observation recording rate of 15 s and others 30 s. The GPS data were processed independently in PPP mode to estimate ZTD using goGPS v1.0 beta1 as the processing software package. goGPS is a MATLAB based GNSS processing software (Realini and Reguzzoni, 2013; Herrera et al., 2016), developed for kinematic applications originally but can also fit quasi static applications. In PPP mode (Zumberge et al., 1997) it can be used to estimate ZTD parameters for meteorological applications (Barindelli et al., 2018; Krietemeyer et al., 2018; Ssenyunzi et al., 2019). The parameters used for the processing of the GPS data can be found in Table 2.

The PWV is estimated by employing meteorological data measured directly at the GPS site and from the ECMWF re-analysis. For each GPS site, the meteorological data is interpolated to the GPS height (Gendt et al., 2004). The ZHD at the GPS sites is then calculated according to the Saastamoinen model (Saastamoinen, 1972).

$$ZHD = \frac{0.0022768 P_{GPS}}{1 - 0.00266\cos 2\phi - 0.00000028h} \tag{2}$$

where h is the height of the surface above the geoid (in metres) and ϕ is the latitude of the station. P_{GPS} is the corresponding air pressure at the station in hPa. The air pressure

Table 2
GPS data processing options.

Processing method	goGPS
Processing mode:	Multi epoch joint least squares adjustment
Sampling interval:	30 s
Frame of reference:	ITRF2008
Antenna PCO/PCV model:	IGS08.ATX
ZTD random walk regularization:	0.015 m/$\sqrt{h}$
ZTD gradients random walk regularization:	0.0015 m/$\sqrt{h}$
Solid earth corrections:	Solid earth tides, ocean loading induced earth tides, and polar motion induced earth tides according to IERS 2010
Ocean loading:	FES 2004
Ionospheric model:	Ionospheric-free
Satellite elevation cut-off:	10 degrees
GNSS observables:	GPS iono free using L1 and L2 band
Other corrections:	Phase wind up, Shapiro delay
Ambiguity:	Float
Mapping function:	VMF gridded mapping function
Apriori ZHD and ZWD:	VMF gridded mapping function
Orbits and satellite clocks:	International GNSS Service (IGS) final products

P_{GPS} at the GPS site in Eq. (2) is obtained by vertically interpolating the surface pressure P_s using the barometric formula:

$$P_{GPS} = P_s e^{-\left(\frac{M_d g \Delta h}{RT}\right)} \tag{3}$$

where T is the standard temperature of the atmosphere at sea level, Δh is height difference between the GPS antenna and the meteorological sensor, R(8.31432 Jmol^{-1}K^{-1}) is the universal gas constant for air, M_d (0.02896 kg mol^{-1}) is the molar mass of dry air and g (9.80665 ms^{-2}) is the gravitational acceleration.

In the troposphere, the temperature is related to the elevation change using the following linear relation:

$$T_{GPS} = T_s - L\Delta h \tag{4}$$

where T_{GPS} and T_s are the surface air temperature at the GPS site and meteorological sensor in Kelvin, L is the temperature lapse rate. By analyzing the ERA5 temperature profiles, the mean temperature lapse rates, over the 4 years of ERA5 data of this altitude interval, at different stations were computed.

$$L = \frac{\Delta T}{\Delta h} \tag{5}$$

where ΔT is the difference between the interpolated model temperature at the station height and the temperature at the lowest model level, Δh is the difference between the model station height and the model surface height. The mean values of L applied in this research, for the five stations, are shown in Table 5. The L for NURK (1.49 K/km) was found to be positive, the vertical interval was though very small (about 60 m), and values show a large scatter. Also, according to Hagemann et al. (2003), for a few occasions, it is possible that the lapse rate is positive. Following that work, this could cause an erroneous computation of temperature and hence PWV. However in this study here, the results of GPS PWV were very similar when compared to those computed using the standard lapse rate of −6.5 K/km.

After the ZTD and ZHD are calculated, the zenith wet delay (ZWD) is also obtained from:

$$ZTD = ZHD + ZWD \tag{6}$$

Then ZWD is converted into PWV using the conversion factor Q (Bevis et al., 1994):

$$PWV = Q \cdot ZWD \tag{7}$$

The conversion factor is calculated using measurements of surface temperature. Askne and Nordius (1987), determined the conversion factor as

$$Q = \frac{10^6}{\rho_v R_v \left(\frac{k_3}{T_m} + k_2'\right)} \tag{8}$$

where ρ_v is the density of water and R_v is the specific gas constant of water vapour (461.5 Jkg^{-1} K^{-1}). The T_m is the weighted mean temperature of the atmosphere given by Davis et al. (1985) as

$$T_m = \frac{\int_h \frac{P_v}{T} dh}{\int_h \frac{P_v}{T^2} dh} \quad (9)$$

In this study, T_m is calculated from the vertical profiles of P_v, the partial pressure of water vapor and T, the temperature derived from ERA5 model.

The T_m can also be estimated from the station temperature T_s (in K) observations using a linear empirical relationship of T_m and T_s such as that developed by Bevis et al. (1992).

$$T_m = 0.72T_s + 70.2 \quad (10)$$

The Bevis et al. (1992) model was developed based on 8718 radiosonde data profiles from 13 sites in the United States over 2 year period (1990–1991).

The Bevis relationship has been widely used in derivation of PWV/IWV such as (Karabati et al., 2011; Xu et al., 2012; Mengistu et al., 2015; Alshawaf et al., 2017). However, Ross and Rosenfeld (1997) and Wang et al. (2005) discovered that the Bevis relationship is limited especially in the tropics. This implies that Bevis model cannot represent the actual climatic condition globally. Efforts have been made to improve the global T_m models such as that developed by Yao et al. (2014). They carried out a study to adjust the Bevis model where 135 globally distributed radiosonde stations were utilized over 10-year period and derived the following global T_m - T_s relationship

$$T_m = 0.8116T_s + 43.69 \quad (11)$$

2.5. Precipitation and SST data

As mentioned, SST and precipitation influences the climate in the investigated region. Precipitation data is obtained from version 2.3 of the Global Precipitation Climatology Project (GPCP) monthly precipitation dataset from 1979 to present (Huffman et al., 2009), which combines gauge observations and satellite data into 2.5 ° × 2.5 ° global grids available at: http://iridl.ldeo.columbia.edu/SOURCES/.NASA/.GPCP/.V2p3/.CDR/.precip/. The observed sea surface temperature is from version 3b of the National Oceanic and Atmospheric Administration (NOAA) National Climate Data Center (NCDC) Extended Reconstructed Sea Surface Temperature (ERSST) (Smith et al., 2008), which is a globally gridded monthly dataset with a spatial resolution of 2.0 ° × 2.0 ° from 1854 to the present. The data can be obtained online from: http://iridl.ldeo.columbia.edu/expert/SOURCES/.NOAA/.NCDC/.ERSST/.version3b/.sst/.

3. Results and discussion

3.1. Comparison of pressure and temperature from ERA5 Reanalysis and meteorological sensors

The pressure and temperature values at the 13 GPS stations over the investigated region were estimated using ERA5 reanalysis model levels interpolated to station heights.

Table 3
Mean Bias (MnB) and RMSE between the interpolated and measured meteorological parameters from ERA5 reanalysis surface meteorological data at 5 stations.

Site	Pressure (hPa)		Temperature (K)		
	MnB	RMSE	MnB	RMSE	No. data
ARSH	−1.01	1.06	0.33	0.88	1190
DODM	0.75	0.79	0.62	1.07	814
MBEY	−0.96	0.98	0.36	1.19	632
MTVE	−0.06	0.28	0.36	1.10	827
NURK	−0.53	0.47	0.35	0.94	854
Mean	**−0.36**	**0.72**	**0.40**	**1.04**	

To validate the accuracy and performance of the ERA5 pressure and temperature, these parameters were compared to data from the meteorological sensors at the 5 GPS stations. Taking sensor meteorological data (MET) as reference, Table 3 presents the mean bias and RMSE values of pressure and temperature differences between the ERA5 estimates and the 5 GPS stations sensor data for a period of at least 2 years (2013 to the beginning of 2015). Figs. 2 and 3 show the scatter plots for pressure and temperature values. The overall mean bias and RMSE for pressure values are −0.36 hPa and 0.72 hPa respectively, with correlation coefficients ranging from 0.976 to 0.996. The absolute biases of the interpolated pressure as presented in Table 3 are all below 1.6 hPa and according to the error propagation law, this would produce approximately 3.6 mm of error in ZHD (Jiang et al., 2016), which is equated to about 0.5 mm bias in the resulting GPS PWV (Zhaoyang et al., 2019).

From Table 3, the mean bias values from the sensor and ERA5 temperature differences at the stations are under 0.7 K with a maximum value at 0.62 K (DODM). This exhibits a good agreement between the two datasets. The overall mean bias and RMSE of the interpolated surface temperature at the 5 stations are 0.40 K and 1.04 K respectively. Zhaoyang et al. (2019) also reported the range of the seasonal bias from the ERA5 reanalysis temperature data as 0.40 K over the coastal regions of China.

3.2. Comparison of the different T_m calculations

In this study, we compared T_m obtained from ERA5 Eq. (8), Bevis et al. (1992) regression Eq. (9) and Yao et al. (2014) regression Eq. (10). The surface temperature, vertical profiles of water vapor pressure and temperature (in Eq. (8)) from ERA5 were employed and Table 4 summarizes the statistics of T_m comparisons among the three data sets using 4 years (2013–2016) data. The T_m from ERA5 is considered to be the most accurate among the T_m estimates at the sites. The difference between the ERA5 and Bevis T_m at all the sites shows that the overall mean bias and RMSE are 1.12 K and 2.05 K respectively. However the mean bias

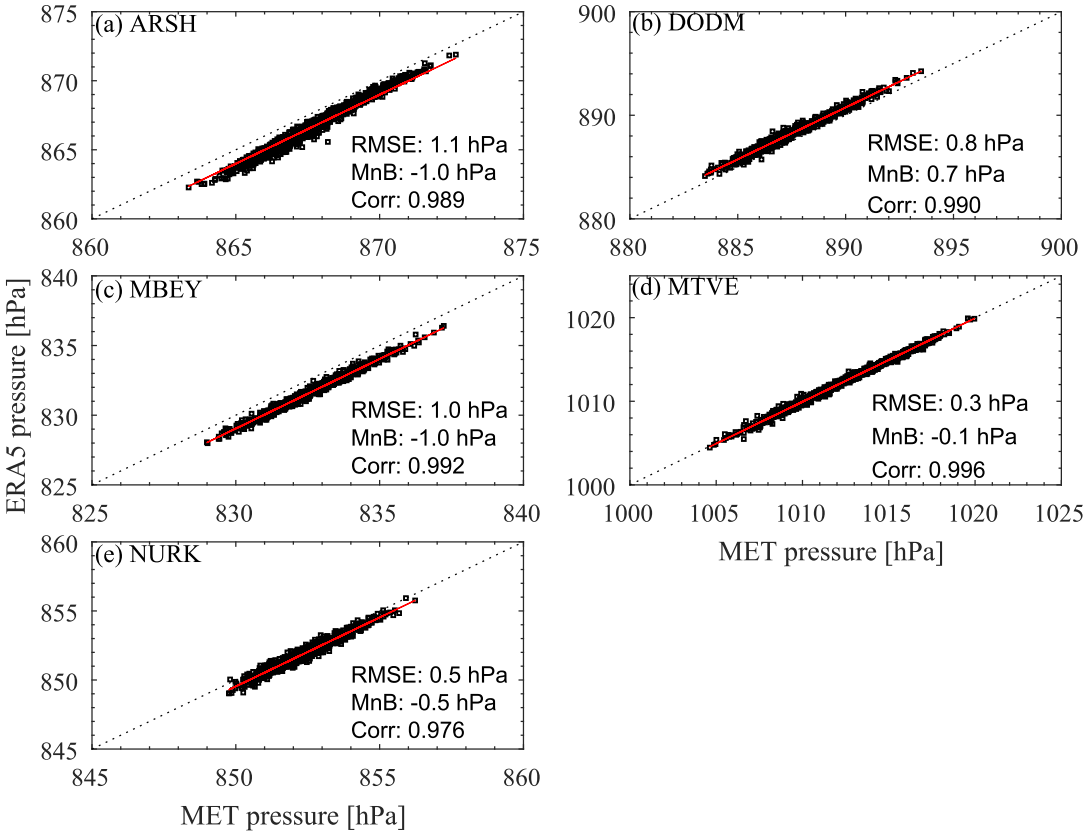

Fig. 2. Scatter plots of ERA5 pressure versus meteorological sensors pressure for the five stations that have meteorological sensors co-located.

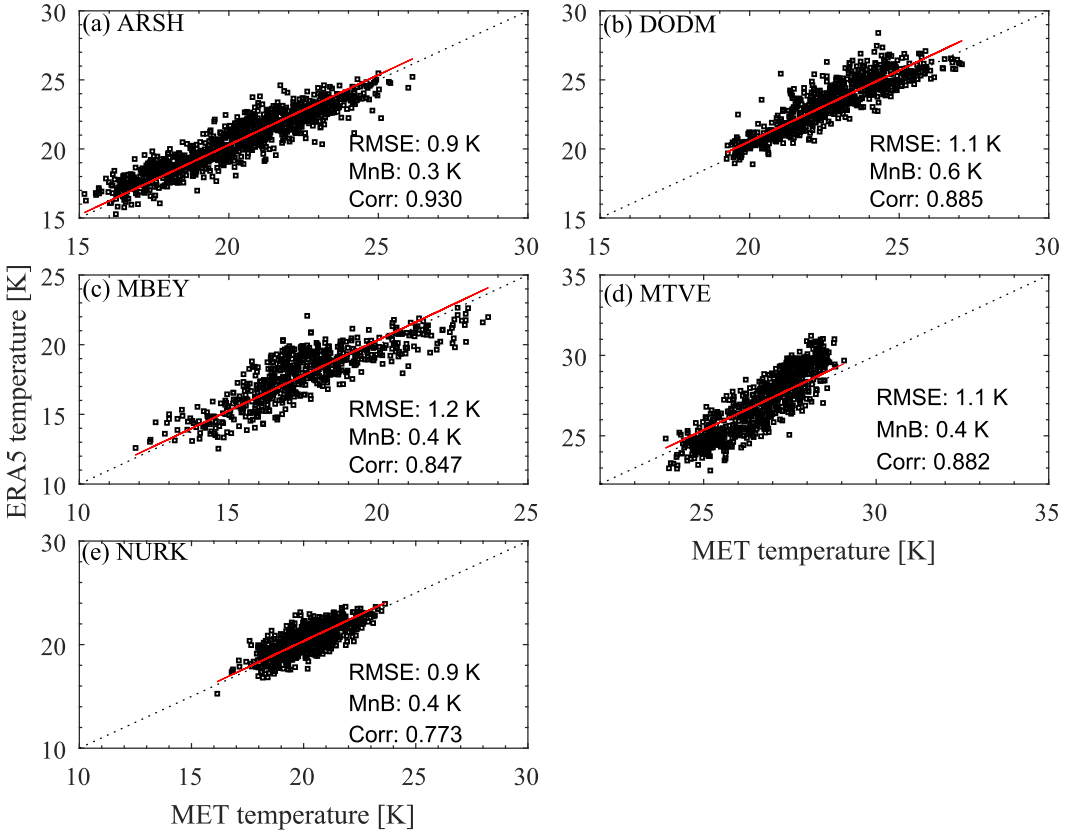

Fig. 3. Scatter plots of ERA5 temperature versus meteorological sensors temperature for the five stations that have meteorological sensors co-located.

Table 4
Statistical comparison between ERA5 T_m, Bevis T_m and Yao T_m.

Site	ERA5 T_m-Bevis T_m(K)		ERA5 T_m-Yao T_m(K)	
	MnB	RMSE	MnB	RMSE
ARSH	0.73	1.58	0.36	1.56
DODM	0.55	1.69	−0.04	1.68
KFNY	2.15	2.77	2.13	2.82
MAL2	2.62	2.93	1.68	2.14
MBAR	−0.49	1.32	−1.02	1.60
MBEY	2.41	1.11	0.97	2.45
MOIU	−0.41	1.21	−0.45	1.26
MTDK	2.24	4.47	1.64	4.64
MTVE	2.38	2.92	1.43	2.26
NURK	−0.03	1.28	−0.40	1.35
RCMN	0.00	1.17	−0.34	1.24
SNGC	0.85	1.82	−0.34	1.24
TNDC	1.61	2.33	0.93	2.00
Mean	**1.12**	**2.05**	**0.50**	**2.02**

at individual stations varies between −0.49 K and 2.62 K. The RMSE values at individual sites vary between 1.11 K and 4.47 K.

The difference between the ERA5 and Yao T_m at all the sites shows that the overall mean bias and RMSE are 0.50 K and 2.05 K respectively. The bias at individual stations varies between −1.02 K and 2.13 K with most sites below 1.7 K whereas the RMSE values at individual sites vary between −1.24 K and 4.64 K.

From both comparisons, MTDK has the highest RMSE (4.47 and 4.64 K) values and this could be attributed to the extrapolation errors in the vertical profiles of data employed. This station has the biggest height difference of −582.20 m in altitude between the station and the surface ECMWF interpolated model level as compared to other stations (see Table 1).

Generally the difference between ERA5 and Yao T_m at all the sites shows a decrease in the overall mean bias by 0.62 K, and RMSE by 0.03 K as compared to the difference between ERA5 and Bevis T_m. The slightly better performance of the Yao T_m, with respect to ERA T_m as compared to Bevis relationship might be explained by the highly variable geography and climate of the East African tropical region compared to United States which is used in the Bevis calculation.

Comparing this study with the study by Namaoui et al. (2017), a lower limit of the mean bias between Bevis T_m and ECMWF reanalysis T_m (−0.03 K) is observed in this study as compared to 2 K for Algeria. This might be explained by the differences in climate. Algeria belongs to subtropical zone where the dominant climate is hot and dry (Namaoui et al., 2017). The higher accuracy of the T_m from this study could also be due to the use of high resolution ERA5 reanalysis dataset as compared to the ERA-Interim Namaoui et al. (2017) applied.

The overall RMSE in the T_m estimated by the T_m- T_s relationships from Bevis and Yao with respect to ERA5 T_m in the region under study, is within the range reported by other studies e.g (Davies and Watson, 1998; Liou et al., 2001; Baltink et al., 2002; Bokoye et al., 2003).

Table 5
Summary of the temperature lapse rate (L), correlation, MnB and RMSE of GPS ERA5 PWV with respect to GPS MET PWV at the five GPS stations.

Site	L(K km^{-1})	corr	MnB (mm)	RMSE (mm)	No. Data
ARSH	−8.53	0.992	-0.59	0.90	1103
DODM	−13.39	0.998	−0.01	0.46	796
MBEY	−12.03	1.00	−0.32	0.35	632
MTVE	−10.51	1.00	−0.17	0.25	827
NURK	1.49	1.00	−0.16	0.19	843
Mean			**−0.26**	**0.44**	

3.3. Comparison between GPS ERA5 PWV and GPS MET PWV

The daily GPS PWV determined based on ERA5 interpolated pressure, temperature (GPS ERA5 PWV) and ERA5 T_m at the 5 stations is compared with the GPS MET PWV derived from sensor pressure and temperature. The GPS ERA5 PWV values are taken as reference values in assessing the GPS MET PWV.

The results in Table 5 show that the two datasets highly correlate, with correlation coefficients ranging between 0.992 and 1.00.

It is observed that at individual sites, biases are in the range of −0.59 mm and −0.01 mm. The bias values of PWV are all negative, showing that the GPS ERA5 PWV estimates are lower than those from GPS MET PWV. The RMSE values at the 5 stations are in the range of 0.19 mm–0.46 mm with exception of ARSH station with a RMSE value of 0.90 mm. The comparisons between the two datasets clearly demonstrate that GPS ERA5 and GPS MET PWV are almost similar.

The higher RMSE at ARSH was due to the observed L2 data loss in some ARSH data files, exposing the results to a very active ionosphere over this low latitude area. The loss of GPS L2 data reduces the accuracy of the GPS ZTD (Jiang et al., 2016), and this further leads to a decrease in the GPS PWV accuracy.

The results in this study, with the exception of ARSH, are in agreement with the study by Wang et al. (2017). They also observed that the RMSE are in the range of 0.1–0.7 mm in the tropics when the PWV computed using reanalysis T_m was compared to PWV (Bevis). The results are also in agreement with the study by Zhaoyang et al. (2019). They showed that data based on GPS PWV products that used interpolated parameters from ERA5 were very close to those of meteorological observations, with average mean bias of ±0.4 mm and RMSEs below 0.5 mm in most areas. These data also strongly agreed with radiosonde observations. Therefore, the accuracy of deriving GPS PWV using pressure and temperature estimates from ECMWF reanalysis data in the region under study

is reliable compared with GPS PWV derived from surface/sensor meteorological data because their errors are in the range of the other quality GPS-derived PWV.

3.4. Comparison between ERA5 and GPS ERA5 PWV

Daily mean PWV data from ERA5 (ERA5 PWV) is compared with GPS ERA5 PWV at the 13 stations, to represent the distribution of the GPS sites over the East African tropical region. Fig. 4 and Table 6 show the scatter plots and statistics of the two datasets. High correlation exists between the datasets as demonstrated in figures with correlation coefficients ranging between 0.943 and 0.988. However, the correlation coefficients for stations near the equator (in region between latitudes 4 °S and 4 °N) are observed to be slightly lower (0.943–0.970) than those in the southern region between latitudes 12 °S and 4 °S (0.980–0.988). This could probably be due to the limitations of the ECMWF re-analysis to represent the high spatial and temporal PWV variability in humid regions and the complex terrain of the region under study.

Table 6
ERA5 PWV minus GPS ERA5 PWV comparison table.

Staion Id	corr	MnB (mm)	RMSE (mm)	No. Data
ARSH	0.943	0.74	1.98	1148
DODM	0.981	0.46	1.55	815
KFNY	0.987	0.27	1.35	959
MAL2	0.970	−0.26	1.75	1430
MBAR	0.949	−0.26	1.44	1175
MBEY	0.985	0.93	1.64	805
MOIU	0.950	0.95	1.65	1229
MTDK	0.980	1.20	2.25	1102
MTVE	0.985	0.28	1.89	837
NURK	0.947	−0.19	1.48	845
RCMN	0.953	0.35	1.53	930
SNGC	0.988	0.16	1.42	947
TNDC	0.986	0.55	1.70	736
Mean		**0.40**	**1.66**	

From Table 6, the mean bias values at individual stations between ERA5 and GPS ERA5 PWV, are in the range −0.26 to 1.20 mm with an overall average bias value of 0.40 mm. The RMSE values are in the range 1.35 mm to

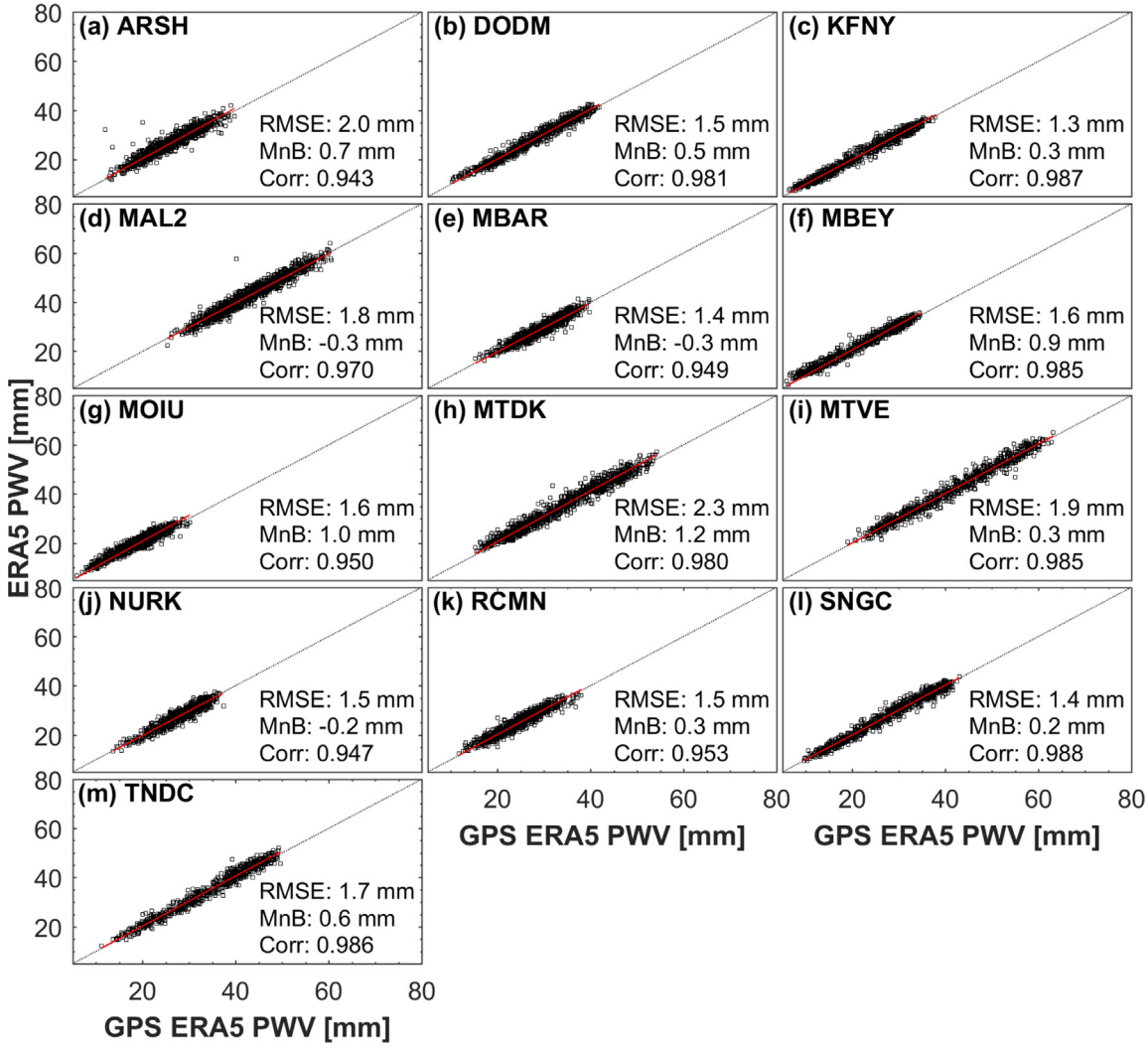

Fig. 4. Scatter plots of ERA5 versus GPS ERA5 PWV for the 13 stations.

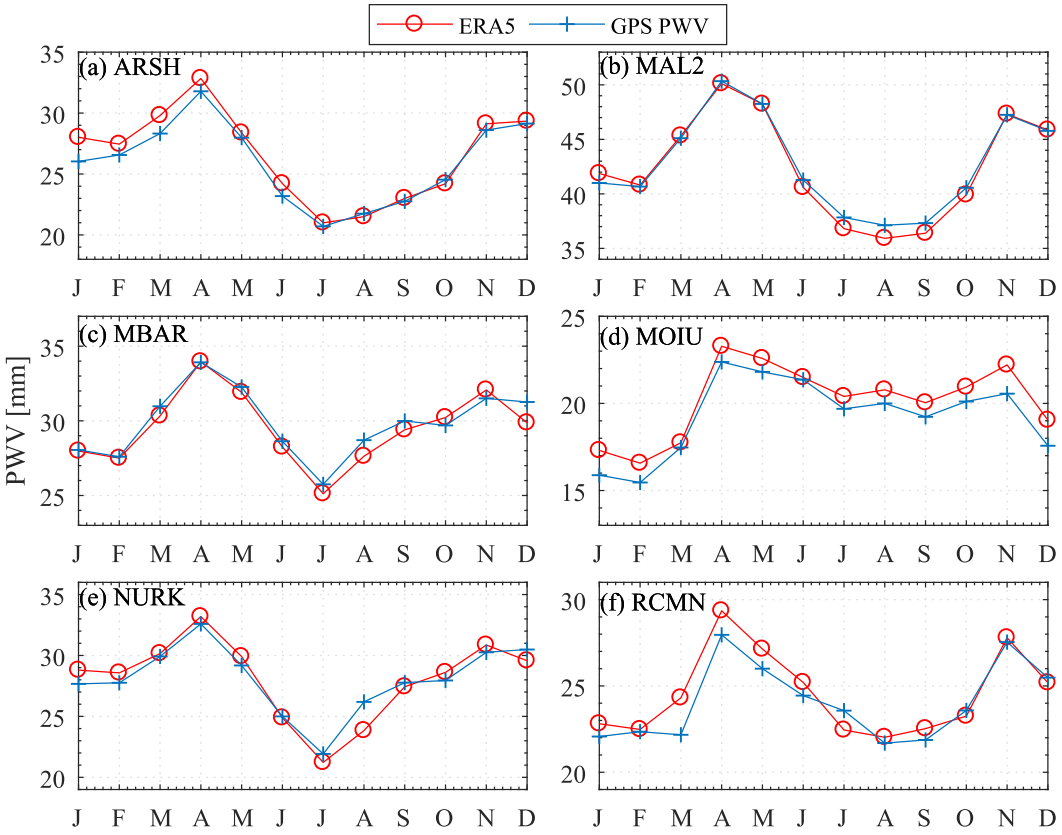

Fig. 5. The seasonal PWV cycle as captured by ERA5 and GPS for stations in the region between latitudes 4 °S and 4 °N from 2013 to 2016.

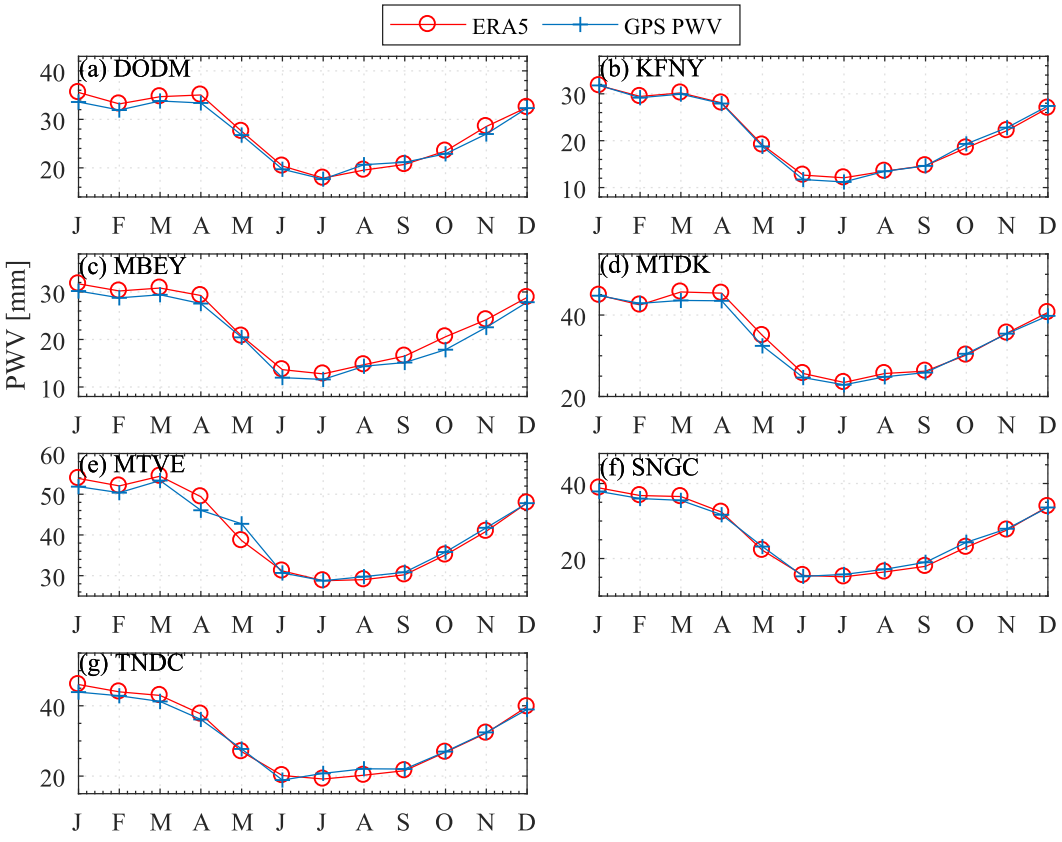

Fig. 6. The seasonal PWV as captured by ERA5 and GPS for stations in the region between latitudes 12 °S and 4 °S from 2013 to 2016.

approximately 2.25 mm with overall average value of 1.66 mm. The higher mean bias and RMSE values at Mtandika (MTDK) station are attributed to the large height difference between the lowest ECMWF model level and the GPS antenna height which is −582.20 m (see Tables 1 and 6). The large height difference causes a significant error in the height reduction of the pressure and PWV (Vey et al., 2010) and also in ERA5 T_m. The errors are assumed to be generated by altitude extrapolation method.

Generally, the observed ERA5 PWV - GPS ERA5 PWV RMS errors (1.35–2.25 mm) observed in this study are in the range of 1 mm to 3 mm, consistent with previous studies such as (Li et al., 2003; Gendt et al., 2004; Deblonde et al., 2005; Wang et al., 2007). However, comparison with studies from Africa e.g. Mengistu et al. (2015) and Namaoui et al. (2017) show the results in this study to be relatively lower. This may probably be due to accuracies of surface meteorological observations applied in these studies and the variations in the climatic conditions. For example, some of the meteorological observations applied by Mengistu et al. (2015) were derived from GPT while the study carried out by Namaoui et al. (2017) was in a subtropical zone.

3.5. Variation of PWV over East Africa tropical region

Figs. 5 and 6 show monthly averages of the PWV from 2013 to 2016. It is observed that the PWV seasonal variability over the East African tropical region is characterized by different behaviors as demonstrated in Figs. 5 and 6 depending on the area in which the station is located. Stations near the equator i.e. in region between latitudes 4 °S and 4 °N exhibited a different behavior from stations in the region between latitudes 12 °S to 4 °S. It can be noticed that there is a good agreement between the monthly averages of the two datasets. It is observed that most of the peaks in the PWV time series caused by rapid changes in the water vapor content are captured well.

From Fig. 5, the average values, display an increase in PWV from minimum values in February up to maximum values in April at all the stations within that region after which the values slightly decrease to minimum values between July and September. The average values of PWV then increase gradually to another maximum values in November. However, the maximum average values of PWV in April are higher than those observed in November. The two datasets exhibit a double peak in PWV, in

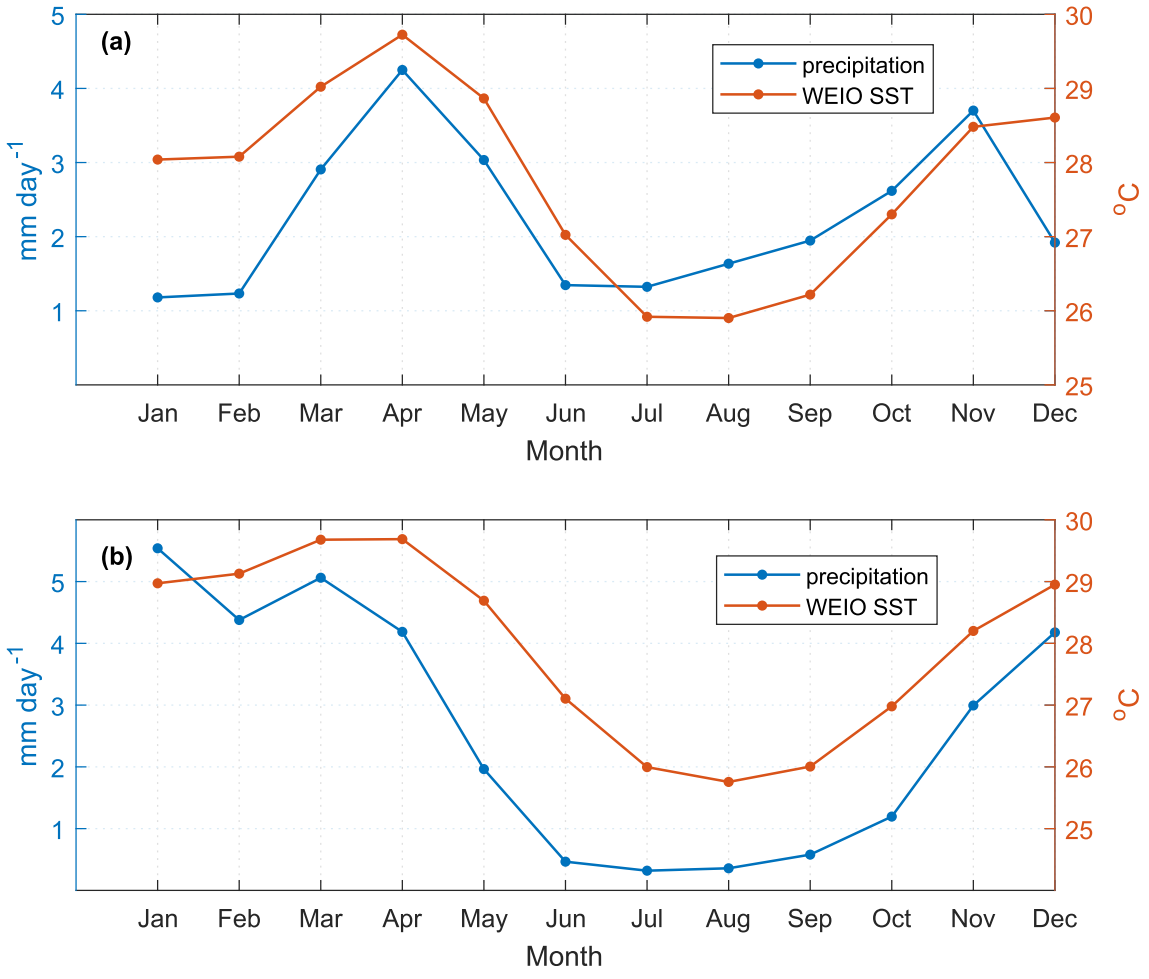

Fig. 7. East African precipitation annual cycle and annual cycle of SST over the Western equatorial Indian Ocean (WEIO) for years 2013–2016 for regions (a) between latitudes 4 °S and 4 °N and (b) between latitudes 12 °S and 4 °S.

Table 7
The average and seasonal mean PWV (mm) as determined from the 13 ground-based GPS receivers used in this study.

Site	av.PWV	MAM	JJA	SON	DJF
ARSH	26.06	29.34	21.81	25.31	27.21
DODM	28.68	31.38	19.26	23.76	32.69
KFNY	22.33	25.41	11.98	18.83	29.38
MAL2	42.56	47.83	38.57	41.57	42.26
MBAR	30.04	32.43	27.80	30.46	28.96
MBEY	22.16	25.66	12.33	18.43	29.02
MOIU	19.27	20.57	20.33	19.98	16.29
MTDK	34.68	39.53	23.81	30.35	42.28
MTVE	43.51	47.33	29.45	35.86	50.04
NURK	28.36	30.50	24.38	28.64	28.56
RCMN	24.00	25.43	23.28	24.42	23.37
SNGC	28.12	30.26	16.72	23.35	35.54
TNDC	33.63	34.90	20.34	27.08	41.83

April - May and October - November, for stations in the region between latitudes 4 °S and 4 °N. The same findings were also reported by Bock et al. (2007a). They observed that stations located near the equator exhibit a double peak in PWV, in April - May and October - November. Comparing Figs. 5–7, there is a strong correlation between precipitation and PWV. Fig. 7(a) shows precipitation and the Western Indian Ocean sea-surface temperature (WEIO SST) for the region near the equator (between latitudes 4 °S and 4 °N). This figure compared with Fig. 5 shows that April and November with high peaks of PWV values are associated with the peaks of the rainy seasons in this region. Also according to Abraha et al. (2015), rainfall is associated to water vapour content in the atmosphere however, the presence of high quantities of water vapour does not mean that there will always be rainfall. The equatorial East African region has double-peak regimes with rain in most parts by March to May (long rain) and October to December (short rain) seasons (Ndomeni et al., 2018). This seasonal cycle is strongly created by north–south movement of the intertropical convergence zone (ITCZ) across the region (Anyah et al., 2006). This might also be the reason for the double peak in PWV, in April- May and October - November. The lower average PWV values in November as compared to April might be due to the Western Indian Ocean SST being lower in October-November-December as it might also be the cause of short rains in the same season as observed in Fig. 7(a). Yang et al. (2015) also reported that the OND season receives low rainfall amount as compared to the MAM season due to the Western Indian Ocean sea-surface temperature (SST) being lower in OND which results into a slightly drier and more stable atmosphere.

From Fig. 6, the average values of PWV decrease gradually from the highest values in January to the lowest values between June and September, then gradually increase to maximum values in December. The inter-annual variability of PWV for stations in the region between latitudes 12 °S and 4 °S, has one marked peak in December - January for the two datasets. This region as presented in Fig. 7(b) is also characterized by unimodal rainfall distribution spanning from November to April. The same findings were also reported by Favre et al. (2011). It is part of southern Tanzania and exhibits single peak regimes with a summer maximum corresponding to the ITCZ because of its location in the southern hemisphere (Camberlin, 2018).

Figs. 5 and 6 have clearly exhibited fluctuations in the PWV datasets across the different months and stations, with one or two minimums or maximums, probably describing the two distinct seasons in East African tropical region. Generally PWV variations exhibited significant seasonal dependence, with larger values in April and November for a region near the equator (the region between latitudes 4 °S and 4 °N), and in December-January for the region between latitudes 12 °S and 4 °S. As observed in Figs. 5–7, changes in PWV can be used to predict precipitation. In a study carried out by Hollway and Neelin (2010) about the temporal relations of column water vapour and tropical precipitation, it was also reported that there is an autocorrelation time of PWV compared to precipitation.

The average values of GPS PWV for different seasons are analysed over the East African tropical region, as presented in Table 7. Fig. 8 shows seasonal mean of PWV from ECMWF reanalysis data from 2013 to 2016 for the four seasons. The different seasons considered in this study include March-April-May (MAM), June-July-August (JJA), September-October-November (SON) and December-January-February (DJF). These represent the spring, summer, autumn and winter in the Northern Hemisphere and the autumn, winter, spring and summer in Southern Hemisphere (Jin et al., 2009; Abraha et al., 2015).

From Table 7, the average values of PWV at most GPS sites in the region between 4 °S and 4 °N are maximum in spring season (MAM) with average PWV values ranging between 20.57 mm (MOIU) and 47.83 mm (MAL2). The lowest average values in this region are observed during summer (JJA) with values ranging between 20.33 mm to 38.58 mm. The average values of PWV at GPS sites in the region between 12 °S and 4 °S are maximum in summer season (DJF) with average PWV values ranging between 29.02 mm (MBEY) and 50.04 mm (MTVE). The lowest average values in this region are observed during winter (JJA) with average values ranging between 11.98 mm to 29.45 mm because Southern Tanzania belongs to the southern Hemisphere. The stations within coastal sites (MTVE and MAL2) are also shown in Fig. 8, they show the highest PWV content (above 40 mm) and this is influenced by the low elevation (also see Fig. 9), proximity to the Indian Ocean, the related high temperature and humidity (Abraha et al., 2015) among other factors. Also according to Fig. 8, regions near the Indian Ocean show the highest amount of PWV for all four seasons. Following Fig. 8, there is a consistent low PWV region in all the four seasons, which is mostly in Kenya. This is related to the elevation of that region which is relatively high over 2000 m. According to Fig. 9, the mean PWV values decrease with increasing

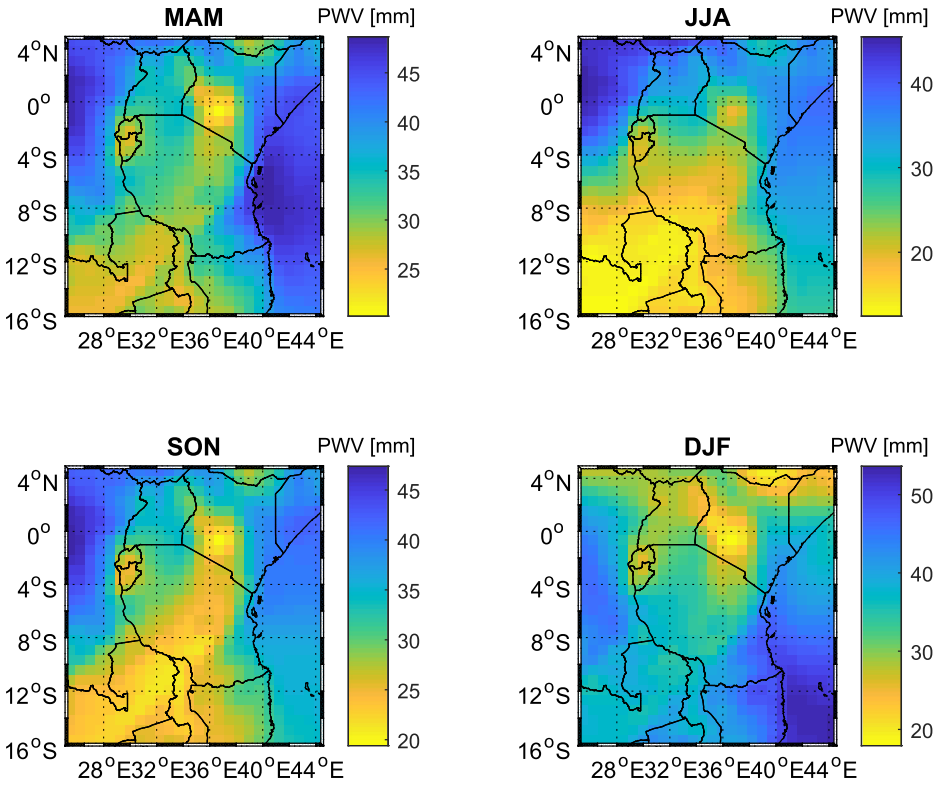

Fig. 8. Spatial and seasonal variations of ECMWF re-analysis PWV for the four seasons over East Africa tropical from 2013 to 2016.

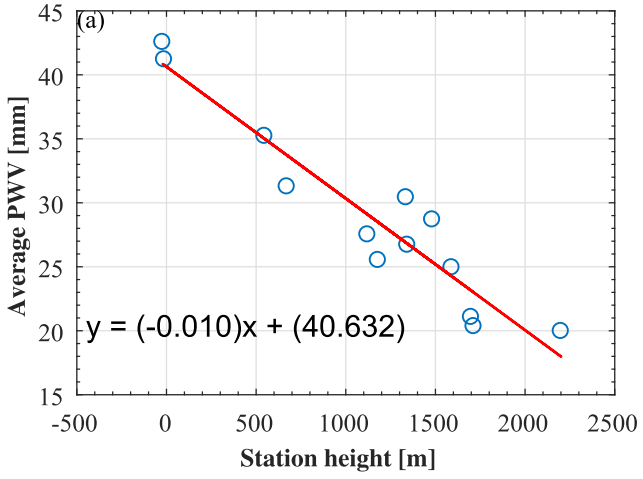

Fig. 9. Plot of average PWV against station elevation.

altitude due to the atmospheric pressure decreasing with the increase in height.

4. Conclusion

Lack of accurate surface pressure and temperature measurements affect the accuracy of the Global Positioning System (GPS) Precipitable Water Vapour (PWV) products. However, NWP dataset can be used as an alternative to obtain the required meteorological parameters necessary for the GPS PWV derivation.

The comparison of sensor surface pressure and temperature and ERA5 pressure and temperature shows an agreement with an overall average RMSE of 0.72 hPa and 1.04 K, respectively. Because interpolation and extrapolation of ERA5 data generated surface meteorological parameters with acceptable accuracies, the study demonstrated that it can serve as a complement to the present ground based GPS meteorological observation networks.

In this study, the T_m results derived from ERA5, the Bevis and Yao T_m - T_s relationships are compared for the period 2013–2016 at the 13 station over the East African tropical region. In comparisons, the T_m derived from ERA5 profile was used as the reference. The bias and RMSE values between ERA5 T_m and Bevis T_m at most of the sites are in the range of −0.49 K to 2.62 K and 1.11 K to 4.47 K with an average mean bias and RMSE of about 1.12 and 2.05 K respectively. The bias and RMSE values between ERA5 T_m and Yao T_m at most of the sites are in the range of −1.02 K to 2.13 K and 1.24 K to 4.64 K with an average bias and RMSE of about 0.50 and 2.02 K respectively. The RMS errors in this study indicate that the Yao T_m - T_s relationship slightly outperforms Bevis T_m - T_s at most of the stations.

The performance of PWV from sensor pressure and temperature (GPS MET PWV) at the 5 stations equipped with meteorological sensors compared to GPS PWV computed from interpolated ERA5 pressure and temperature values (GPS ERA5 PWV) was investigated. The GPS ERA5 PWV was used as the reference for the performance

assessment of the two sets of GPS PWVs. The RMSE values at the sites for the two datasets are in the range of 0.19 mm–0.90 mm with an average RMSE of 0.44 mm.

The comparison between the PWV determined from ERA5 (ERA5 PWV) and GPS ERA5 PWV at the 13 GPS stations was also performed. The comparison shows that the RMSE values at most of the sites for the two datasets are in the range of 1.35 mm–2.25 mm with an average RMSE of 1.66 mm.

The PWV seasonal variability over the East African region exhibited two different behaviors with stations in the regions between latitudes 4 °S and 4 °N and between latitudes 12 °S to 4 °S having unique but similar behavior. Stations in region between latitudes 4 °S and 4 °N were found to have a seasonal variation with highest values observed during spring and lowest values during summer. Stations in region between latitudes 12 °S and 4 °S were found to have a seasonal variation with highest values observed during winter and lowest values during summer. However, further analysis about the variability and trends in PWV and some of the processes influencing them over the East African tropical region is required.

Acknowledgments

The research project was partly funded by the European Union's Horizon 2020 research and innovation programme under grant agreement No. 776691 (TWIGA). R. C. Ssenyunzi acknowledges the financial support from Busitema University. The authors also acknowledge Copernicus C3S/CAMS, CDDIS, UNAVCO, GPCP and NCDC/NOAA for providing the data used in this study.

References

Abraha, K.E., Lewi, E., Masson, F., Boy, J., 2015. Spatial-temporal variations of water vapour content over Ethiopia: a study using GPS observations and the ECMWF model. GPS Solut.

Alshawaf, F., Hinz, S., Mayer, M., Meyer, F.J., 2015. Constructing accurate maps of atmospheric water vapor by combining interferometric synthetic aperture radar and GNSS observations. J. Geophys. Res. 120, 1391–1403.

Alshawaf, F., Balidakis, K., Dick, G., Heise, S., Wickert, J., 2017. Estimating trends in atmospheric water vapour and temperature time series over Germany. Atmos. Meas. Tech. 10, 3117–3132.

Anyah, R.O., Semazzi, F.H., Xie, L., 2006. Simulated physical mechanisms associated with climate variability over Lake Victoria Basin in East Africa. Mon. Weather Rev. 134, 3588–3609.

Askne, J., Nordius, H., 1987. Estimation of tropospheric delay for microwaves from surface weather data. Rad. Sci. 22, 379–386.

Baltink, H.K., van der Marel, H., van der Hoeven, A.G.A., 2002. Integrated atmospheric water vapor estimates from a regional GPS network. J. Geophys. Res. 107 (D3), 4025. https://doi.org/10.1029/2000JD000094.

Barindelli, S., Realini, E., Venuti, G., Fermi, F., Gatti, A., 2018. Detection of water vapor time variations associated with heavy rain in northern italy by geodetic and low-cost gnss receivers. Planets Space. 70, 28.

Bennitt, G.V., Jupp, A., 2012. Operational assimilation of GPS zenith total delay observations into the met office numerical weather prediction models. Mon. Weather Rev. 140, 2706–2719.

Bevis, M., Businger, S., Herring, T.A., Rocken, C., Anthes, R.A., Ware, R.H., 1992. GPS meteorology: Remote sensing of atmospheric water vapour using the Global Positioning System. J. Geophys. Res. 97, 15787–15801.

Bevis, M., Businger, S., Chiswell, S., 1994. GPS meteorology: mapping zenith wet delays onto precipitable water. J. Appl. Meteorol. 33, 379–386.

Bock, O., Keil, C., Richard, E., Flamant, C., Bouin, M.N., 2005. Validation of precipitable water from ECMWF model analyses with GPS and radiosonde data during the MAP SOP.Q.J. Roy. Meteor. Soc. 131, 3013–3036.

Bock, O., Bouin, M.N., Walpersdorf, A., Lafore, J.P., Janicot, S., Guichard, F., Agusti-Panareda, A., 2007b. Comparison of ground-based GPS precipitable water vapour to independent observations and NWP model reanalyses over Africa. Q.J.R. Meteorol. Soc. 133, 2011–2027.

Bock, O., Guichard, F., Janicot, S., Lafore, J.P., Bouin, M.N., Sultan, B., 2007a. Multiscale analysis of precipitable water vapour over Africa from GPS data and ECMWF analyses. Geophys. Res. Lett. 34, 1–6.

Bock, O., Willis, P., Lacarra, M., Bosser, P., 2010. An intercomparison of zenith tropospheric delays derived from DORIS and GPS data. Adv. Space Res. 46, 1648–1660.

Bock, O., Guichard, F., Meynadier, R., Gervois, S., Agusti Panareda, A., Beljaars, A., Boone, A., Nuret, M., Redelsperger, J.L., Roucou, P., 2011. The large-scale water cycle of the West African monsoon. Atmosph. Sci. Lett. 12, 51–57.

Boehm, J., Heinkelmann, R., Schuh, H., 2007. A global model of pressure and temperature for geodetic applications. J. Geod. 81, 679–683.

Bokoye, A.I., Royer, A., Oneill, N.T., Clich, P., McArthur, L.J.B., Teillet, P. M., Fedosejevs, G., Theriault, J.M., 2003. Multisensor analysis of integrated atmospheric water vapor over Canada and Alaska. J. Geophys. Res. 108 (D15), 4480. https://doi.org/10.1029/2002JD002721.

Buehler, S.A., Stman, S., Melsheimer, C., Holl, G., Eliasson, S., John, V. O., Blumenstock, T., Hase, F., Elgered, G., Raffalski, U., Nasuno, T., Satoh, M., Milz, M., Mendrok, J., 2012. A multi instrument comparison of integrated water vapour measurements at a high latitude site. Atmos. Chem. Phys. 12, 10925–10943.

Camberlin, P., 1997. Rainfall anomalies in the source region of the Nile and their connection with the Indian summer monsoon. J. Clim. 10, 1380–1392.

Camberlin, P., 2018. Oxford Research Encyclopedia of Climate Science. climatescience.oxfordre.com.

Campanelli, M., Mascitelli, A., San, P., Dimoz, H., Estells, V., Federico, S., Iannarelli, A.M., Fratarcangeli, F., Mazzoni, A., Realini, E., Crespi, M., Bock, O., Martnez-Lozano, A., Dietrich, S., 2018. Precipitable water vapour content from ESR/SKYNET sun-sky radiometers:validation against GNSS/GPS and AERONET over three different sites in Europe. Atmos. Meas. Tech. 11, 81–94.

Combrink, A., Combrinck, W., Moraal, H., 2004. Near real-time detection of atmospheric water vapour using the SADC GPS network. South African J. Sci. 100, 436–442.

Dach, R., Lutz, S., Walser, P., 2015. Bernese GNSS Software Version 5.2. 854.

Davies, O.T., Watson, P.A., 1998. Comparisons of integrated precipitable water vapor obtained by GPS and radiosondes. Electron. Lett. 34 (7), 645–646.

Davies, T.D., Vincent, C.E., Beresford, A.K.C., 1985. July-August rainfall in West-Central Kenya. J. Clim. 5, 17–33. The limnology, climatology, and paleoclimatology of the East African lakes, 25–56.

Davis, J.L., Herring, T.A., Shapiro, I.I., Rogers, A.E.E., Elgered, G., 1985. Geodesy by radio interferometry: effects of atmospheric modeling on estimates of baseline length. Radio Sci. 20, 1593–1607.

Deblonde, G., Macpherson, S., Mireault, Y., Heroux, P., 2005. Evaluation of GPS precipitable water over Canada and the IGS network. J. Appl. Meteorol. 44, 153–166.

Dietrich, S.V.R., Johnsen, K.P., Miao, J., Heygster, G., 2004. Comparison of tropospheric water vapour over Antarctica derived from AMSUB data, ground-based GPS data and the NCEP/NCAR reanalysis. J. Meteorol. Soc. Jpn. 82, 259–267.

Durre, I., Vose, S., Wuertz, D., 2006. Overview of the integrated global radiosonde archive. J. Clim. 19, 53–68.

Favre, A., Stone, D., Cerezo, D., Philippon, N., Abiodun, B. 2011, Diagnostic of monthly rainfall from CORDEX simulations over Africa: Focus on the annual cycles. In: On the Coordinated Regional Climate Downscaling Experiment-CORDEX, Trieste, Italy, World Climate Research Program, Proc. Int. Conf.

Gendt, G., Dick, G., Reigber, C., Tomassini, M., Liu, Y., Ramatschi, M., 2004. Near real time GPS water vapor monitoring for numerical weather prediction in Germany. J. Meteor. Soc. Jpn. 82, 361–370.

Gerding, M., Christoph, R., Marion, M., Roland, N., 2004. Tropospheric water vapour soundings by lidar at high Arctic latitudes. Atmos. Res. 71, 289–302.

Hagemann, S., Bengtsson, L., Gendt, G., 2003. On the determination of atmospheric water vapor from GPS measurements. J. Geophys. Res., 108

Herrera, A.M., Suhandri, H.F., Realini, E., Reguzzoni, M., Clara de Lacy, M., 2016. gogps: open-source matlab software. GPS solut. 20, 595–603.

Herring, T.A., King, R.W., Floyd, M.A., 2015. GAMIT Reference Manual Release 10.6. 168.

Hersbach, H., Dee, D., 2016. ERA5 reanalysis is in production. ECMWF Newsletter No. 147, 7.

Hollway, C., Neelin, J., 2010. Temporal relations of column water vapor and tropical precipitation. J. Atmos. Sci., 1091–1105

Huffman, G.J., Adler, R.F., Bolvin, D.T., Gu, G., 2009. Improving the global precipitation record: GPCP version 2.1. Geophys. Res. Lett. 36, L17808.

Jiang, P., Ye, S., Chen, D., Liu, Y., Xia, P., 2016. Retrieving precipitable water vapor data using GPS zenith delays and global reanalysis data in China. Remote Sens. 8, 396.

Jin, S., Luo, O.F., Gleason, S., 2009. Characterization of diurnal cycles in ZTD from a decade of global GPS observations. J. Geod. 83, 537–545. https://doi.org/10.1007/s00190-008-0264-3.

Karabati, A., Weber, R., Haiden, T., 2011. Near real-time estimation of tropospheric water vapour content from ground based GNSS data and its potential contribution to weather now-casting in Austria. Adv. Space Res. 47, 1691–1703.

King, M.D., Menzel, W.P., Kaufman, Y.J., Tanr, D., Gao, B.C., Platnick, S., Ackerman, S.A., Remer, L.A., Pincus, R., Hubanks, P.A., 2003. Cloud and aerosol properties, precipitable water, and profiles of temperature and water vapor from MODIS. IEEE Trans. Geosci. Remote Sens. 41, 442–458.

Koulali, A., Ouazar, D., Bock, O., Fadil, A., 2011. Study of seasonal scale atmospheric water cycle with ground-based GPS receivers, radiosondes and NWP models over Morocco. Atmos. Res. 41 (104–105), 273–291.

Krietemeyer, A., ten Veldhuis, M., Marel, H., Realini, E., Giesen, N., 2018. Potential of cost-efficient single frequency gnss receivers for water vapor monitoring. Rem. Sens. 10, 1493.

Kuwahara, T., Mizuno, A., Nagahama, T., Maezawa, H., Morihira, A., Toriyama, N., Murayama, S., Matsuura, M., Sugimoto, T., Asayama, S., Mizuno, N., Onishi, T., Fukui, Y., 2008. Ground based millimeter-wave observations of water vapour emission (183 GHz) at Atacama, Chile. Adv. Space Res. 42, 1167–1171.

Köpken, C., 2001. Validation of integrated water vapor from numerical models using ground-based GPS, SSM/I, and water vapor radiometer measurements. J. Appl. Meteor. 40, 1105–1117.

Lewis, H., 2007. Geodesy calculations in ROPP. GRAS SAF Report 02.

Li, X., Dick, G., Ge, M., Wickert, J., Bender, M., 2014. Real-time GPS sensing of atmospheric water vapour: Precise point positioning with orbit, clock, and phase delay corrections. Geophys. Res. Lett. 41, 3615–3621.

Li, Z., Muller, J.P., Cross, P., 2003. Comparison of precipitable water vapor derived from radiosonde, GPS, and moderate-resolution imaging spectroradiometer measurements. J. Geophys. Res. 108, 46–51.

Liou, Y.A., Teng, Y.T., Van Hove, T., Liljegren, J.C., 2001. Comparison precipitable water observation in the near tropics by GPS, microwave radiometer, and radiosondes. J. Appl. Meteorol. 40, 5–15.

Luo, X., Heck, B., Awange, J.L., 2013. Improving the estimation of zenith dry tropospheric delays using regional surface meteorological data. Adv. Space Res. 52, 2204–2214.

Maghrabi, A.H., 2009. Parameterization of a simple model to estimate monthly global solar radiation based on meteorological variables, and evaluation of existing solar radiation models for Tabouk, Saudi Arabia. Energy Conserv. Manage. 50, 2754–2760.

Maghrabi, A.H., Clay, R., 2010. Precipitable water vapour estimation on the basis of sky temperatures measured by a single-pixel IR detector and screen temperatures under clear skies. J. Meteorol. Appl. 17, 279–286.

Mahoney, M.J., 2001. A discussion of various measures of altitudes. http://mtp.jpl.nasa.gov/notes/.

Mengistu, T.G., Blumenstock, T., Hase, F., 2015. Observations of precipitable water vapour over complex topography of Ethiopia from ground-based GPS, FTIR, radiosonde and ERA-Interim reanalysis. Atmos. Meas. Tech. 8, 3277–3295.

Moustafa, T., 1992. The hydrological cycle and its influence on climate. Nature 359.

Namaoui, H., Kahlouche, S., Belbachir, A., Van Malderen, R., Brenot, H., Pottiaux, E., 2017. GPS water vapour and its comparison with radiosonde and ERA-Interim data in Algeria. Atmos. Sci. 41, 623–634.

Ndomeni, W., Cattani, E., Merino, A., Levizzani, V., 2018. An observational study of the variability of East African rainfall with respect to sea surface temperature and soil moisture. Q.J.R. Meteorol Soc. 144, 384–404.

Nicholson, S.E., 1996. A review of climate dynamics and climate variability in Eastern Africa. In: Johnson, T.C., Odada, E.O. (Eds.).

Ohtani, R., Naito, I., 2000. Comparison of GPS-derived precipitable water vapour with radiosonde observations in Japan. J. Geophys. Res. 105, 6917–26929.

Realini, E., Reguzzoni, M., 2013. gogps: open source software for enhancing the accuracy of low-cost receivers by single-frequency relative kinematic positioning. Meas. Sci. Technol. 24, 115010.

Ross, R.J., Rosenfeld, S., 1997. Estimating mean weighted temperature of the atmosphere for Global Positioning System applications. J. Geophys. Res. 102 (D18), 21719–21730.

Saastamoinen, J., 1972. Atmospheric correction for the troposphere and stratosphere in radio ranging of satellites. In: Geophysical Monogram Series, American Geophysical Union, Band 15, Washington, D.C., pp. 247–251.

Sharifi, M.A., Khaniani, A.S., Joghataei, M., 2015. Comparison of GPS precipitable water vapour and meteorological parameters during rainfalls in Tehran. Meteorol. Atmos. Phys.

Sibylle, V., Dietrich, R., Rlke, A., Fritsche, M., Steigenberger, P., Rothacher, M., 2010. Validation of precipitable water vapor within the NCEP/DOE reanalysis using global GPS observations from one decade. J. Clim. 23, 1675–1695.

Slingo, J., Spencer, H., Hoskins, B., Berrisford, P., Black, E., 2005. The meteorology of the Western Indian Ocean, and the influence of the East African Highlands. Philosoph. Trans. Roy. Soc. London Mathe., Phys. Eng. Sci. 363, 25–42.

Smith, M., Reynolds, W., Peterson, C., Lawrimore, J., 2008. Improvements to NOAAs historical merged land ocean surface temperature analysis (1880–2006). J. Climate 21, 2283–2296.

Ssenyunzi, R.C., Oruru, B., Dujanga, F.M., Realini, E., Barindelli, S., Tagliaferro, G., van de Giesen, N., 2019. Variability and accuracy of Zenith Total Delay over the East African Tropical Region. Adv. Space Res. 64, 900–920. https://doi.org/10.1016/j.asr.2019.05.027.

Thiery, W., Davin, E.L., Panitz, H.J., Demuzere, M., Lhermitte, S., Van Lipzig, N., 2015. The impact of the African Great Lakes on the regional climate. J. Clim. 28, 4061–4085.

Vedel, H., Huang, X.Y., 2004. Impact of ground based GPS data on numerical weather prediction. J. Meteorol. Soc. Jpn. 82, 459–472.

Vey, S., Dietrich, R., Rulke, A., Fritsche, M., 2010. Validation of precipitable water vapor within the NCEP/DOE reanalysis using global GPS observations from one decade. J. Clim. 2 (23), 1675–1695.

Wang, J., Liangying, Z., Aiguo, D., 2005. Global estimates of water-vapour-weighted mean temperature of the atmosphere for applications. J. Geophys. Res. 110, D21101. https://doi.org/10.1029/2005JD006215.

Wang, J., Zhang, L., Dai, A., Hove, T.V., Baelen, J.V., 2007. A near-global, 2-hourly data set of atmospheric precipitable water from groundbased GPS measurements. J. Geophys. Res. 2007.

Wang, X., Zhang, K., Wu, S., Fan, S., Cheng, Y., 2017. Water vapour weighted mean temperature and its impact on the determination of precipitable water vapour and its linear trend. J. Geophys. Res. Atmos. 121, 833–852.

Xu, G., Cui, C., Wan, R., Lai, Wan, X., Fu, Z., Feng, G., 2012. Applicability of methods for estimating GPS precipitable water in the Qinghai-Tibet Plateau. J. Atmos. Solar Terr. Phys. 89, 76–78.

Yang, W., Seager, R., Cane, M.A., Lyon, B., 2015. The annual cycle of east African precipitation. J. Clim. 28, 2385–2404.

Yao, Y.B., Zhang, B., Xu, C.Q., Yan, F., 2014. Improved one/multi-parameter models that consider seasonal and geographic variations for estimating weighted mean temperature in ground-based GPS meteorology. J. Geod. 88, 273–282.

Yuan, L.L., Anthes, A.R., Ware, H.R., Rocken, C., Bonner, D.W., Bevis, M.G., Businger, S., 1993. Sensing climate change using the global positioning system. J. Geophys. Res. 98, 14925–14937.

Yunck, T.P., Liu, C.H., Ware, R., 2000. A history of GPS sounding. Terr. Atmos. Ocean Sci. 11, 1–20.

Zhang, Y., Xu, J., Yang, N., Lan, P., 2018. Variability and trends in global precipitable water vapor retrieved from COSMIC radio occultation and radiosonde observations. Atmos. 174, 3117–3132.

Zhaoyang, W., Zhe, X., Xinghua, Z., Qiuhua, T., Dongxu, Z., Weikang, Sun, 2019. GPS-based precipitable water vapour retrieval and variability using measured and global reanalysis data in the coastal regions of China. Int. J. Remote Sensing 40 (23), 8857–8878.

Zumberge, J.F., Heflin, M.B., Jefferson, D.C., Watkins, M.M., Webb, F. H., 1997. Precise point positioning for the efficient and robust analysis of GPS data from large networks. J. Geophys. Res 102, 5005–5017.